Journal of Fluorescence (2019) 29:665–672
https://doi.org/10.1007/s10895-019-02377-1

ORIGINAL ARTICLE

Synthesis, Luminescence, and Energy Transfer Properties of YPO_4:Gd^{3+}, Eu^{3+} and YP_3O_9:Sm^{3+}, Eu^{3+} Phosphors

S. Hachani [1] · L. Guerbous [2]

Received: 1 February 2019 / Accepted: 10 April 2019 / Published online: 27 April 2019

Abstract

This work is concerned with the search for new luminescent materials emitting in the orange-red color. We have synthesized YPO_4 doped with Gd^{3+}0.25% and/or Eu^{3+}0.50% by hydrothermal method and YP_3O_9 doped with Sm^{3+}0.25% and/or Eu^{3+}0.50% by ultraphosphate decomposition reaction. Phase purity was checked by FTIR and XRD. Excitation and emission spectra and fluorescence decay measurements were recorded at room temperature (RT). Emission spectra allow to determine the site symmetry of rare earth (RE^{3+}) in the crystallographic structure of matrices. Weak Eu^{3+} emission is detected from YPO_4:Gd^{3+}, Eu^{3+} under excitation at 273 nm. Sm^{3+} levels were detected in excitation spectrum of YP_3O_9:Sm^{3+}, Eu^{3+} monitoring Eu^{3+} principal emission at 618 nm. Excited states lifetimes of Gd^{3+} and Sm^{3+} sensitizers (S) decrease from mono-doped to co-doped matrices indicating an Energy transfers (ET) from S to Eu^{3+} with a rate higher than 19%.

Keywords Phosphate · Hydrothermal · Flux · Luminescence · Energy transfer · Eu^{3+}

Introduction

In the framework of research of new orange-red phosphors with quantum efficiency (QE) higher than 1 for Hg-free fluorescent lamps and plasma display panels (PDP), ET from Gd^{3+} to Eu^{3+} in YPO_4 and from Sm^{3+} to Eu^{3+} in YP_3O_9 are studied. Quantum Cutting (QC) which is a process of ET and cross relaxation (CR) between ions, leads to QE higher than 1 because of the emission of two photons against the absorption of one photon [1]. QC based on (Gd^{3+}, Eu^{3+}) couple of ions where Eu^{3+} is the activator (A), was first successfully studied in $LiGdF_4$ by Wegh [2]. Then, it was widely studied in fluorides and other materials [3, 4]. In this process, we report $Gd^{3+} \rightarrow Eu^{3+}$ ET which consists of $^8S_{7/2} \rightarrow {}^6I_J$ Gd^{3+} excitation, then ^6P_J (Gd^{3+}) $\rightarrow {}^5H_J$ (Eu^{3+}) ET. Finally, $^6P_J \rightarrow {}^8S_{7/2}$ and $^5D_0 \rightarrow {}^7F_J$ transitions respectively of UV and red emissions. The choose of YPO_4 is due to its physico-chimical properties. It is a stoichiometric matrix characterized by large band gap equal to 8.6 eV [5] and high thermal stability (up to 1450 °C [6]). The crystal structure is chains constituted alternatively of YO_8 dodecahedra and PO_4 tetrahedra. Rare earth (RE^{3+}) ions occupy one type of site and the minimal distance between them is equal to 0.3755 nm [7]. YPO_4 co-doped with Tb^{3+}-Yb^{3+} or Tm^{3+}-Yb^{3+} is near–infrared QC (NIR-QC) phosphor with QE > 172% [4]. Moreover, luminescent nanomaterials using YPO_4 as host have been widely used in displays, cathode ray tube, and high-pressure mercury lamp, etc. [8]. To our knowledge, QC based on (Sm^{3+}, Eu^{3+}) couple of ions where Sm^{3+} and Eu^{3+} are respectively S and A, was only studied in YPO_4, LaP_5O_{14} and LaP_3O_9 in previous work [7]. $Sm^{3+} \rightarrow Eu^{3+}$ ET is part of this process and it consists of $^6H_{5/2} \rightarrow {}^4I_{9/2}$ excitation. Then $^4G_{5/2}$ (Sm^{3+}) $\rightarrow {}^5D_0$ (Eu^{3+}) ET. Finally, $^4G_{5/2} \rightarrow {}^6H_J$ and $^5D_0 \rightarrow {}^7F_J$ emissions of orange-red photons. The selection of YP_3O_9 is based on the calculation of Sm^{3+} 5d band position which must be above Q level situated at 53000 cm^{-1} [7]. YP_3O_9 is a stoichiometric matrix characterized by a vacuum ultraviolet (VUV) absorption at 145 and 156 nm of $(PO_3)_3^{3-}$ group [9], RE^{3+} ions occupy four types of site and YO_6 octahedra are isolated from each other which leads to high concentration quenching [10]. Moreover, this matrix has a high thermal stability (up to 900 °C) [6, 11]. According to QC conditions [7], A ion concentration must be higher than that of S. Therefore, the double concentration

✉ S. Hachani
ha1souad@yahoo.fr

[1] Laboratory of Physics of Photonics and Multifunctional Nanomaterials, University of Biskra, B.P. 145 RP, 07000 Biskra, Algeria

[2] Laser Department, Nuclear Research Center of Algiers (CRNA), 02 Bd. Frantz Fanon, B.P. 399, 16000 Algiers, Algeria

is considered for both matrices. Additionally, The maximal energy of the phonons (E_{max}) must be low in order to reduce the non- radiative transition probabilities. Although it is not the case in our samples ($E_{max} \sim 1060\ cm^{-1}$ for YPO_4 [12] and $\sim 1100\ cm^{-1}$ for YP_3O_9 [4]), the phosphates matrices doped RE^{3+} have been widely investigated for intended applications [3, 4, 7].

In the field of fluorescent lamps, it is necessary to replace mercury (harmful to the environment) used as a source of UV photons with another rare gas such as Xenon, source of VUV photons. This last gas employed also in PDP, has a low efficiency regarding that of Hg. So, looking for a new VUV-Vis conversion phosphors with QE higher than one, will perform better. As stated earlier, QC process allows to have these efficiencies. In this paper, the aim of constructing such materials which fulfill QC conditions is to study luminescence and ET.

Experimental

Rare Earth Phosphates Synthesis

The basic products used for the preparation of samples are the following: Y_2O_3 (Rhone-Poulenc, 99.99%), Sm_2O_3 (Rhone-Poulenc, 99.99%), Eu_2O_3 (Alfa Aesar, 99.99%), Gd_2O_3 (Péchiney Saint-Gobain, 99.9%), H_3PO_4 (Panreac, 50–51%) and KBr (Shimadzu Corporation). Samples of Gd^{3+} and/or Eu^{3+} doped YPO_4 and Sm^{3+} and/or Eu^{3+} doped YP_3O_9 were prepared by using respectively hydrothermal method and ultraphosphate decomposition reaction.

Hydrothermal Method

Hydrothermal method is based on reaction between RE oxides (stoichiometric ratios), an excess of orthophosphoric acid and a given amount of water at 200 °C during 4 h within a stainless steel autoclave with a 23 ml Teflon chamber. After the reaction was complete, the autoclave was naturally cooled to RT. Finally, the obtained powder was consecutively washed with hot distilled water, dried at 100 °C in the air and finely grounded [3]. The reaction is expressed in the following equation (Eq. 1):

$$\frac{1}{2}(1-x-y)Y_2O_3 + \frac{1}{2}xEu_2O_3 + \frac{1}{2}yGd_2O_3 + H_3PO_4 \rightarrow Y_{1-x-y}Eu_xGd_yPO_4 + \frac{3}{2}H_2O \quad (1)$$
$$(x,y) = (0.005, 0), (0, 0.0025), (0.005, 0.0025)$$

Obtained powders underwent calcinations at 850 °C and 1000 °C during 2 h (the monophosphates are stable until 1450 °C).

Ultraphosphate Decomposition Reaction

LnP_5O_{14} ultraphosphates transform to $Ln(PO_3)_3$ polyphosphates when they are calcined at temperatures ranging between 800 and 900 °C. First, YP_5O_{14} crystals doped with Sm^{3+} and/or Eu^{3+} were prepared using Flux method [3] with 450 °C for 150 h as conditions. Then, transparent crystals of some millimeters were properly grounded to powder. Finally, the ultraphosphate decomposition reaction [11] was used to develop yttrium polyphosphates at 870 °C for 4 h in air atmosphere (according to Agrawal et al. [6], the decomposition temperature is 860 ± 10 °C). The reaction Eq 3. are:

$$\frac{1}{2}(1-x-y)Y_2O_3 + \frac{1}{2}xEu_2O_3 + \frac{1}{2}ySm_2O_3 + 5H_3PO_4 \rightarrow Y_{1-x-y}Eu_xSm_yP_5O_{14} + \frac{15}{2}H_2O \quad (2)$$

$$Y_{1-x-y}Eu_xSm_yP_5O_{14} \rightarrow Y_{1-x-y}Eu_xSm_y(PO_3)_3 + P_2O_5\uparrow \quad (3)$$
$$(x,y) = (0.005, 0), (0, 0.0025), (0.005, 0.0025)$$

Yttrium polyphosphate powders underwent calcinations at 900 °C for 4 h, then 20 h.

Instruments and Techniques

All the synthesized samples have been checked by infrared absorption spectroscopy technique (FTIR) between 4000 and 400 cm^{-1} with a Shimadzu IR-8400S FTIR spectrometer. The purity of compounds was controlled by X-ray diffraction (XRD) using a Bruker D8 Advance spectrometer with CuKα1 radiation (λ = 1.54060 Å). Excitation and emission spectra were recorded using HORIBA Jobin Yvon FluoroMax-4 spectrofluorometer equipped with 150 W ozone-free Xenon arc-lamp. The beam of continuous light (200–950 nm) is focused on the entrance slit of the excitation monochromator. Then, it is directed onto a sample, which emits luminescence. The luminescence is directed into a second, emission monochromator, which selects a band of wavelengths, and manages them towards a detector (R928P photomultiplier tube). The signal from the detector which has a response ranges from 180 to 850 nm, is reported to a system controller and host computer, where the data can be manipulated and presented using FluorEssence software. The spectra were corrected by means of the software. Also, the fluorescence decays were recorded with this spectrofluorometer. All measurements were made at RT, the slits widths were 0.5/0.5, 1/1 and 5 mm/5 mm and J1939 Cut-On filters were used.

Results and Discussion

Structural Characterization

Infrared Spectroscopy

In the orthophosphate YPO_4 of zircon structure (xenotime phase), PO_4 tetrahedron is isolated and has two antisymmetric vibration modes active in infrared. υ_3 mode of P − O stretching appears around 1080 cm^{-1} and υ_4 mode of O − P − O deformation appears in the region from 500 to 650 cm^{-1}. Figure 1 shows the FTIR spectra of YPO_4 doped with Gd^{3+} and/or Eu^{3+}. The band with three humps at 1124, 1070 and 1006 cm^{-1} corresponds to υ_3 mode. The peaks at 648 and 523 cm^{-1} correspond to υ_4 mode. The band and the peak positions are comparable with reported values [8, 12, 13].

Figure 2 shows FTIR spectra of YP_3O_9 doped with Sm^{3+} and/or Eu^{3+}, The absorption bands separated by vertical dashed line and peaked at: 1259/1234, 1192/1178/1167/1097, 1017/945, 772/747/712/684 and 595/540/519/491 cm^{-1} correspond respectively to asymmetric stretching vibrations of OPO (terminal oxygen): ν_{as}(OPO), symmetric stretching vibrations of OPO: ν_s(OPO), asymmetric stretching vibrations of POP (bridging oxygen): ν_{as}(POP), symmetric stretching vibrations of POP: ν_s(POP) and deformation vibrations of phosphate and the stretching vibrations of yttrium oxygen bonds: δ(OPO or POP) & υ(Y-O). These vibrations are assigned to monoclinic polyphosphates with small RE^{3+} ions (Gd–Lu, Y) [14].

X-Ray Diffraction Spectroscopy

The XRD patterns of Y-monophosphates are shown in Fig. 3 . All the peaks are indexed in the tetragonal zircon-type structure with space group $I4_1/amd$ according to the JCPDS 11–0254 file. Concerning Y-polyphosphates purity, all the peaks in Fig. 4 are indexed in the monoclinic system with C space group according to the JCPDS 42–0501 file.

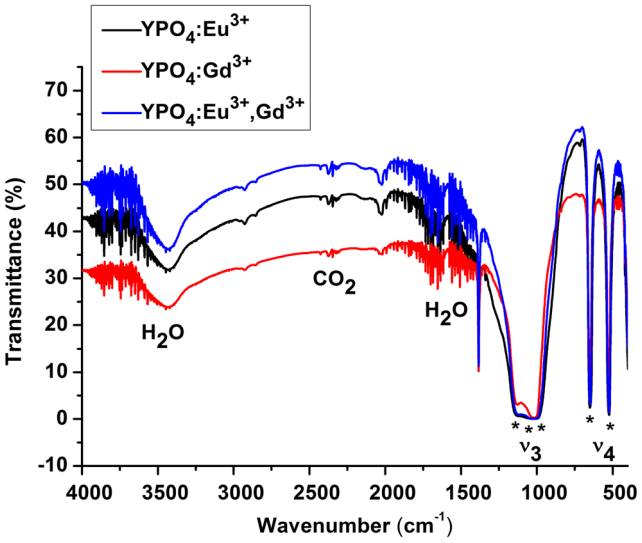

Fig. 1 FTIR spectra of YPO_4 doped with Gd^{3+} and/or Eu^{3+}; (*) xenotime type. Assignments of vibrational bands are indicated

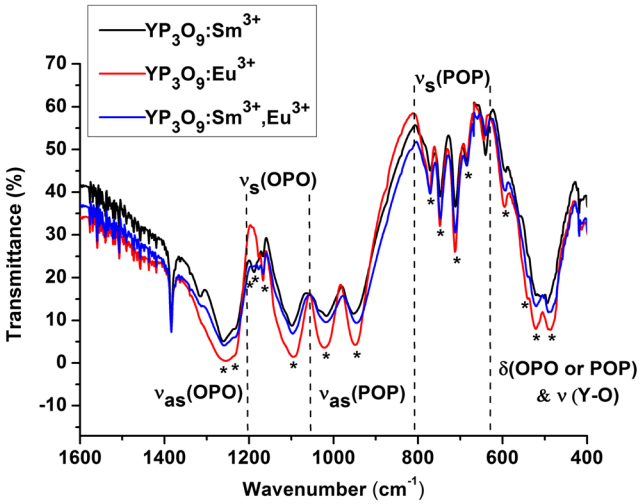

Fig. 2 FTIR spectra of YP_3O_9 doped with Sm^{3+} and/or Eu^{3+}; (*) polyphosphate type. Assignments of vibrational bands are indicated

UV-Visible Spectroscopy

YPO_4:Gd^{3+}0.25%, Eu^{3+}0.50%

YPO_4:Eu^{3+}0.50% excitation spectrum monitoring $^5D_0 \rightarrow {}^7F_2$ principal emission at 618 nm, recorded between 240 and 500 nm using high-pass filter ($\lambda \geq 500$ nm) is presented by black line in Fig. 5. It consists of a broad band situated below 250 nm assigned to Eu^{3+} charge transfer band (CTB) [7] and sharp peaks assigned to Eu^{3+} intra-4f-transitions: $^7F_0$ to $^5I_6$, ^5F_J,^5H_J, $^5D_4$, $^5L_7$, $^5L_6$, $^5D_3$ and $^5D_2$ [3, 7, 15] situated

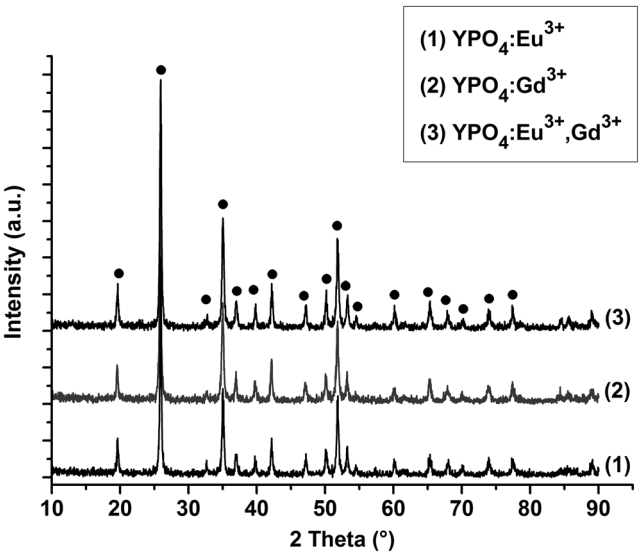

Fig. 3 XRD spectra of YPO_4 doped with Gd^{3+} and/or Eu^{3+}

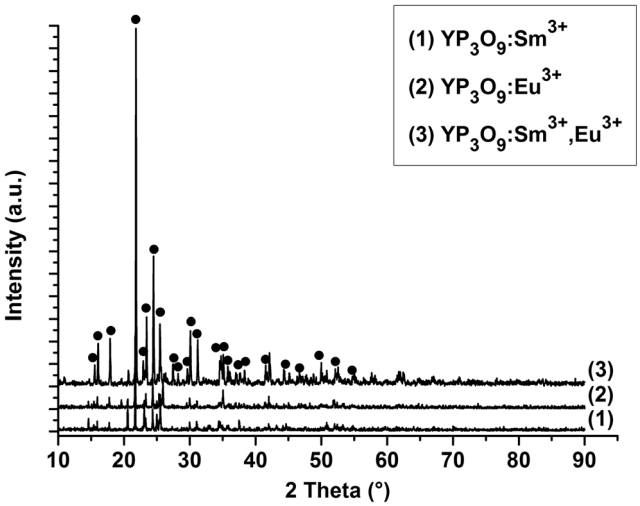

Fig. 4 XRD spectra of YP_3O_9 doped with Sm^{3+} and/or Eu^{3+}

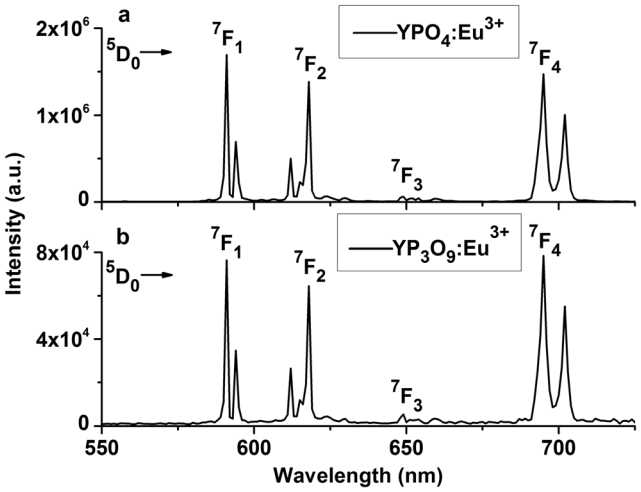

Fig. 6 Emission spectra of (a) $YPO_4:Eu^{3+}$ and (b) $YP_3O_9:Eu^{3+}$ excited into $^5L_6$ level

respectively at 286, 298, 318, 362, 381, 394, 416 and 465 nm. $^5L_6$ level has the highest intensity, Eu^{3+} ion can be excited at this level or at CTB.

The emission spectrum under excitation at 394 nm $^5L_6$ level shown in Fig. 6, is composed by sharp bands situated in the orange-red region and centered at 591, 618, 649 and 695 nm assigned respectively to $^5D_0 \rightarrow {}^7F_1$ Magnetic Dipole Transition (MDT) — its intensity is largely independent of environment, $^5D_0 \rightarrow {}^7F_2$ hypersensitive Electric Dipole Transition (EDT) — its intensity is very strongly dependent on environment, $^5D_0 \rightarrow {}^7F_3$ Forbidden Transition and $^5D_0 \rightarrow {}^7F_4$ EDT — its intensity is dependent on environment, but no hypersensitive. $^5D_0 \rightarrow {}^7F_0$ EDT not detected in our spectrum is usually located between 570 and 585 nm and only observed in C_n, C_{nv} and C_s symmetry [7, 16]. Recalling that the site symmetry in YPO_4 is D_{2d} [12].

In a Centro-symmetric site, the main observed transitions are MDT nature, on the contrary, if the site is non Centro-symmetry the EDT are generally more intense [17]. In the Fig. 6, $^5D_0 \rightarrow {}^7F_1$ MDT is more intense than $^5D_0 \rightarrow {}^7F_{2,4}$ EDT, so D_{2d} site symmetry of Eu^{3+} is Centro-symmetric.

Concerning Gd^{3+} mono-doped YPO_4, UV emission under excitation into ^6I_J level at 273 nm is presented by dashed line in Fig. 7 [3, 15].

$YPO_4:Gd^{3+}0.25\%$, $Eu^{3+}0.50\%$ excitation spectrum monitoring $^5D_0 \rightarrow {}^7F_2$ transition at 618 nm is presented in Fig. 5 (red line). It consists of only Eu^{3+} 4f levels and no Gd^{3+} levels. The no distinction of Gd^{3+} levels is due to its low concentration. In previous work, ^6I_J, ^6P_J and ^6D_J levels of Gd^{3+} were observed in the excitation spectra of $GdPO_4$: $Eu^{3+}x\%$ (x = 1, 7 and 10) [3]. In the case of Gd^{3+}-based phosphate mono-doped with Eu^{3+}, the Gd^{3+} 4f levels appeared in the excitation

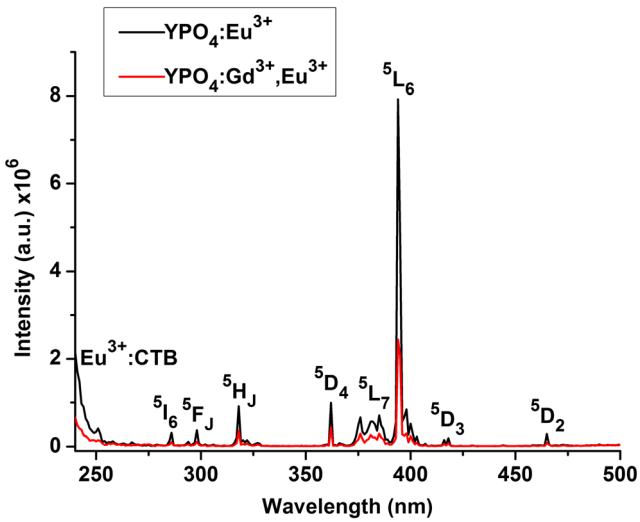

Fig. 5 Excitation spectra of $YPO_4:Eu^{3+}$ and $YPO_4:Gd^{3+}$, Eu^{3+} monitored at 618 nm

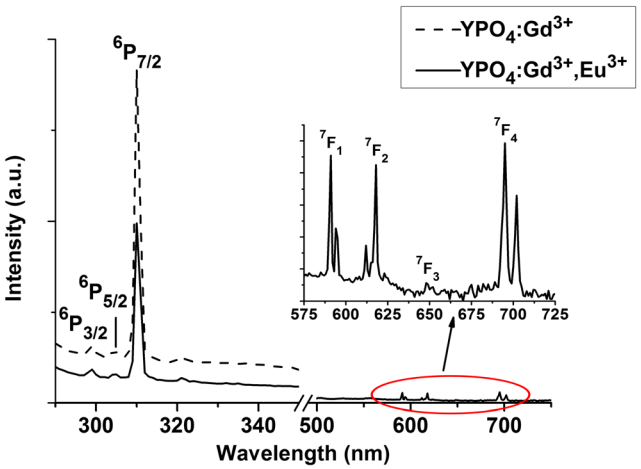

Fig. 7 Emission spectra of $YPO_4:Gd^{3+}$ and $YPO_4:Gd^{3+}$, Eu^{3+} excited into ^6I_J at 273 nm. The inset shows an enlargement of the region from 575 to 725 nm

spectrum monitoring Eu^{3+} emission. Otherwise, these levels are not distinguished for Gd^{3+} low concentration in such phosphates.

To prove $Gd^{3+} \rightarrow Eu^{3+}$ ET, the emission spectrum of YPO_4:Gd^{3+}0.25%, Eu^{3+}0.50% excited into ^6I_J at 273 nm was recorded (solid line, Fig. 7). UV emission is decreased to half compared with Gd^{3+} mono-doped matrix. Weak Eu^{3+} emission corresponding to $^5D_0 \rightarrow {}^7F_J$ is detected, indicating an expected ET occurs. Figure 8 describes the $Gd^{3+} \rightarrow Eu^{3+}$ ET pathway. Noting that no Eu^{3+} emission is observed for mono-doped matrix under excitation at 273 nm.

ET is a type of interaction between RE^{3+} ions. When concentration increases, the distance between RE^{3+} decreases which lead to ET. This later occurs because of S and A 4f energy levels are energetically close to each other. $Gd^{3+} \rightarrow Eu^{3+}$ ET has been pointed out in literature [18]. It was reported that this ET is non-radiative and its rate increases with increasing Eu^{3+} concentration for an optimum concentration of Gd^{3+}.

In YPO_4, Gd^{3+} $^6P_{7/2}$ level situated at 32258 cm^{-1} is close to Eu^{3+} ^5H_J level situated at 31446 cm^{-1} (Fig. 8). Precisely, the gap between these two levels (equal to 812 cm^{-1}) is less than E_{max} which results in a resonant non-radiative energy transfer (NRET). Afterwards a non-radiative decay of ^5H_J to $^5D_0$ which emits in turn simultaneously with Gd^{3+} emission of $^6P_J \rightarrow {}^8S_{7/2}$ transitions.

YP_3O_9: Sm^{3+}0.25%, Eu^{3+}0.50%

The excitation spectrum of Sm^{3+} mono-doped YP_3O_9 monitored at 602 nm ($^4G_{5/2} \rightarrow {}^6H_{7/2}$ principal transition) and recorded between 240 nm and 500 nm using high-pass filter ($\lambda \geq 500$ nm), is presented in Fig. 9. The spectrum contains sharp peaks situated at 304, 317, 332, 343, 360, 374, 390, 401, 404, 414, 419, 438, 461, 465, 473 and 480 nm assigned respectively to $^3H_{9/2}$, $^4F_{11/2}$, $^4D_{7/2}$, P′, O′, $^4K^N_{11/2}$, $^4K^M_{11/2}$, $^4F_{9/2}$, $^4L_{13/2}$, $^6P_{3/2}$, $^6P_{5/2}$, $^4G_{9/2}$, $^4I_{15/2}$, $^4I_{13/2}$, $^4I_{11/2}$ and $^4I_{9/2}$ 4f energy levels [7, 15] and a broad band situated below 260 nm assigned to CTB [19].

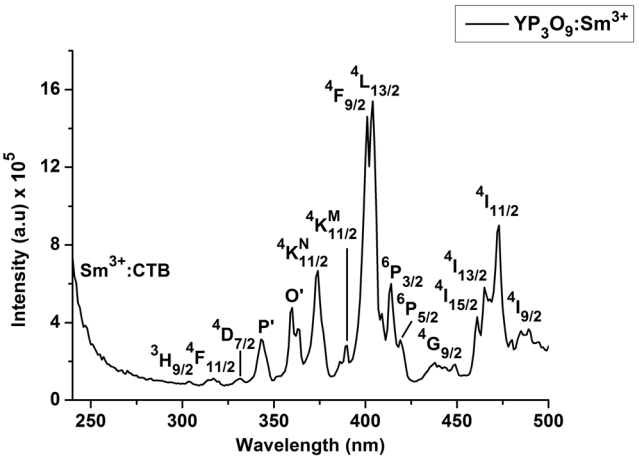

Fig. 9 Excitation spectrum of YP_3O_9:Sm^{3+} monitored at 602 nm

Emission spectrum of this sample, under excitation into $^4L_{13/2}$ level most absorbing (404 nm) presented by black line in Fig. 10, shows four sharp bands centered around 561, 602, 644 and 715 nm corresponding, respectively, to $^4G_{5/2} \rightarrow {}^6H_{5/2}$ MDT, $^4G_{5/2} \rightarrow {}^6H_{7/2}$ partly Magnetic and partly forced Electric Dipole Transition, $^4G_{5/2} \rightarrow {}^6H_{9/2}$ purely EDT sensitive to the crystal field and $^4G_{5/2} \rightarrow {}^6H_{11/2}$ EDT [19]. Generally, the intensity ratio of EDT ($^4G_{5/2} \rightarrow {}^6H_{9/2}$) and MDT ($^4G_{5/2} \rightarrow {}^6H_{5/2}$) of Sm^{3+} ion can be used to understand the symmetry of the local environment of trivalent 4f ions in the host matrix investigated. The asymmetric nature is more prominent when the intensity of the EDT is higher. The ratio value below or above 1.0 indicates the symmetric or

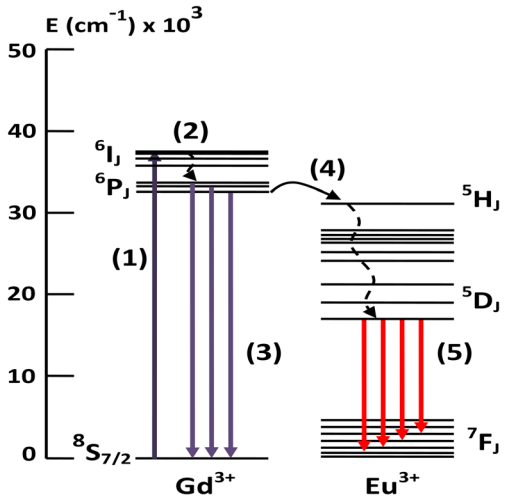

Fig. 8 Energy level diagrams of Gd^{3+} and Eu^{3+} in YPO_4: (1) Gd^{3+} Excitation, (2) Non-radiative decay, (3) Gd^{3+} emission, (4) NRET followed by non-radiative decay of ^5H_J and (5) Eu^{3+} emission. $^5D_0$ energy position is taken from reference [15]

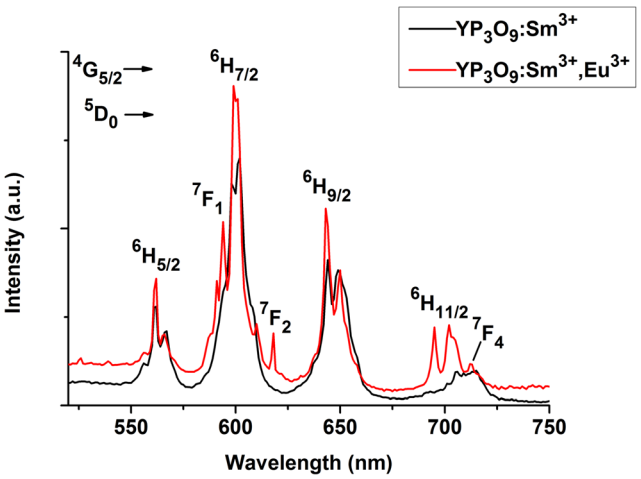

Fig. 10 Emission spectra of YP_3O_9:Sm^{3+} excited into $^4L_{13/2}$ level (black line) and YP_3O_9:Sm^{3+}, Eu^{3+} excited into $^4I_{9/2}$ level (red line)

asymmetric nature of host matrix [19]. According to emission spectrum of $YP_3O_9:Sm^{3+}$, the ratio of intensity between EDT per MDT is above 1.0 which indicates an asymmetric nature of this matrix. Besides, the existence of four RE^{3+} sites in the crystal structure.

Concerning $YP_3O_9:Eu^{3+}$, Excitation spectrum monitoring $^5D_0 \rightarrow {}^7F_2$ transition at 618 nm shown in Fig. 11(black line) is divided into two parts. The first part contains a band situated below 260 nm assigned to CTB [9]. In the second part, there are sharp peaks situated at 285, 298, 318, 362, 376, 382, 394, 416 and 465 nm respectively assigned to $^5I_6$, ^5F_J, ^5H_J, $^5D_4$, ^5G_J, $^5L_7$, $^5L_6$, $^5D_3$ and $^5D_2$ 4f energy levels [7, 15].

$YP_3O_9:Eu^{3+}$ emission spectrum under excitation into $^5L_6$ level presented in the above Fig. 6, is composed by sharp bands centered around 591, 618, 648, 695 nm assigned respectively to $^5D_0 \rightarrow {}^7F_1$ MDT, $^5D_0 \rightarrow {}^7F_2$ EDT, $^5D_0 \rightarrow {}^7F_3$ Forbidden Transition and $^5D_0 \rightarrow {}^7F_4$ EDT [10, 16]. Emission of Eu^{3+} is more intense than that of Sm^{3+} and both are situated in the orange-red region. Also by comparing the spectra of Fig. 6, Eu^{3+} fluorescence in Y-monophosphate is more intense than in Y-polyphosphate.

There are four non-equivalent Eu^{3+} sites in monoclinic YP_3O_9. Two types of sites without inversion symmetry (low symmetry) and two sites with inversion symmetry (high symmetry) [9, 10]. It is known that Eu^{3+} is sensitive to the crystal field environment. When Eu^{3+} occupies the low symmetry sites, its $^5D_0 \rightarrow {}^7F_2$ EDT would be lifted and has the high emissive intensity. Otherwise, if Eu^{3+} occupies the high symmetry sites, the strongest emissive peak of Eu^{3+} is the $^5D_0 \rightarrow {}^7F_1$ allowed transition [9]. The analysis of the spectrum shows that $^5D_0 \rightarrow {}^7F_1$ is the most intense indicating that Eu^{3+} occupies two high symmetric sites.

Excitation spectrum of $YP_3O_9:Sm^{3+}0.25\%$, $Eu^{3+}0.50\%$, monitoring $^5D_0 \rightarrow {}^7F_2$: Eu^{3+} emission at 618 nm shown in Fig. 11 (red line), consists of Sm^{3+} and Eu^{3+} 4f energy levels.

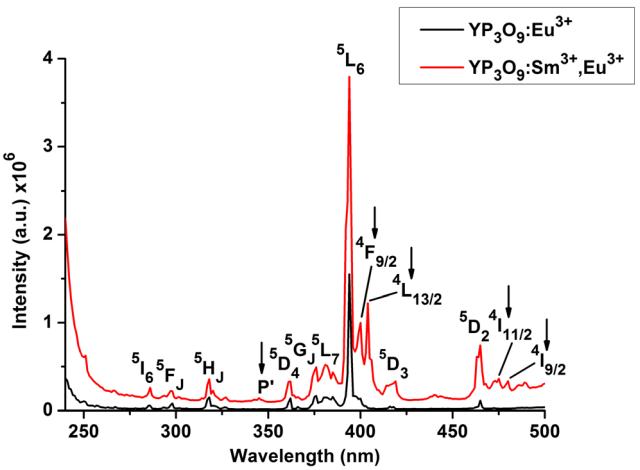

Fig. 11 Excitation spectra of $YP_3O_9:Eu^{3+}$ and $YP_3O_9:Sm^{3+}$, Eu^{3+} monitored at 618 nm

The observation of Sm^{3+} level (P′: 345, $^4F_{9/2}$: 400, $^4L_{13/2}$: 404, $^4I_{11/2}$: 475 and $^4I_{9/2}$: 480 nm) indicates that $Sm^{3+} \rightarrow Eu^{3+}$ ET occurs [7]. The observed peak intensities are weak due to low doping concentrations which leads to low ET. The emission spectrum of co-doped matrix under excitation into $^4I_{9/2}$ Sm^{3+} level at 480 nm shown in Fig. 10, is composed by the emissions of both types of ions (it seems that $^5D_0 \rightarrow {}^7F_3$ transition is hidden by Sm^{3+} emission). The observation of Eu^{3+} emission bands situated at 594 ($^5D_0 \rightarrow {}^7F_1$), 617 ($^5D_0 \rightarrow {}^7F_2$) and 702 nm ($^5D_0 \rightarrow {}^7F_4$) indicates that an expected ET from Sm^{3+} to Eu^{3+} occurs and the pathway is described in Fig. 12. It is noted that no emission was detected in $YP_3O_9:Eu^{3+}$ under excitation at 480 nm. $^4G_{5/2}$ energy position is equal to 17825 cm^{-1} and $^5D_0$ energy position range is 17094–17544 cm^{-1}. It is clear that the gap between these levels is less than E_{max}, so the observed ET is phonon assisted [7].

Fluorescence Decay

The curves in Fig. 13 present the fluorescence decays of $YPO_4:Gd^{3+}0.25\%$ and $YPO_4:Gd^{3+}0.25\%$, $Eu^{3+}0.50\%$ of $^6P_{7/2} \rightarrow {}^8S_{7/2}$ emission at 310 nm under excitation into ^6I_J level at 273 nm. $YPO_4:Gd^{3+}0.25\%$ decay follows a bi-exponential function represented by:

$$I(t) = I_1\, e^{\frac{-t}{\tau_1}} + I_2\, e^{\frac{-t}{\tau_2}} + C \qquad (4)$$

where I is phosphorescence intensity, I_1 and I_2 are the intensities at two different interval times and the corresponding decay times are τ_1 and τ_2, t is time and C is constant. The

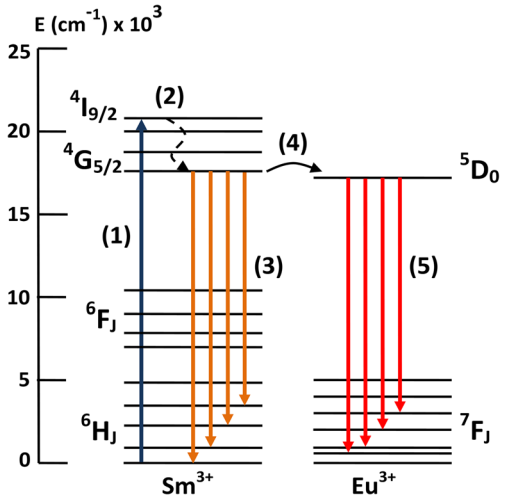

Fig. 12 Energy level diagrams of Sm^{3+} and Eu^{3+}. (1) Excitation into $^4I_{9/2}$ of Sm^{3+} ion, (2) Non-radiative decay of $^4I_{9/2}$ to $^4G_{5/2}$, (3) Sm^{3+} emission of $^4G_{5/2} \rightarrow {}^6H_J$ transitions, (4) NRET — $^4G_{5/2}$ and $^5D_0$ levels are energetically close to each other which results in a resonant non-radiative transfer of excitation energy, (5) Eu^{3+} emission of $^5D_0 \rightarrow {}^7F_J$ transitions. $^5D_0$ energy position is taken from reference [15]

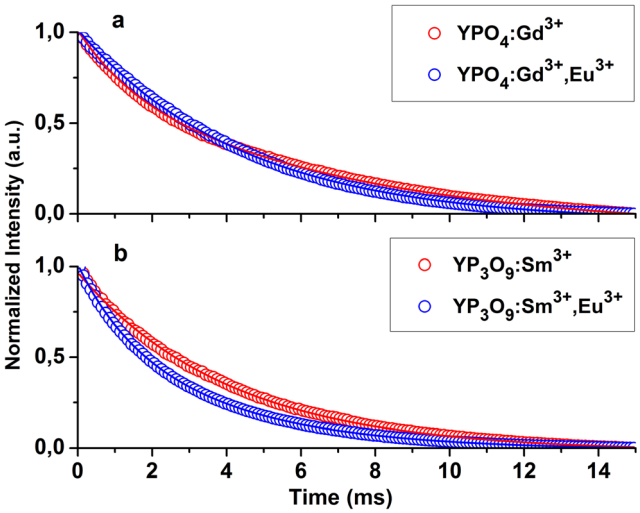

Fig. 13 Fluorescence decays of (**a**) YPO_4:Gd^{3+} and YPO_4:Gd^{3+}, Eu^{3+} at 310 nm emission of Gd^{3+} under excitation into ^6I_J level at 273 nm and (**b**) YP_3O_9:Sm^{3+} and YP_3O_9:Sm^{3+}, Eu^{3+} at 602 nm emission of Sm^{3+} under excitation into $^4I_{9/2}$ level at 480 nm. The circles indicate the experimental data, and the solid lines are fitting curves

average decay time τ_{Gd} is calculated using the Eq. (5) [20]. Table 1 lists the values of S decay times and ET rates in samples, τ_{Gd} is long.

$$\tau_{moy} = \frac{I_1\tau_1 + I_2\tau_2}{I_1 + I_2} \tag{5}$$

Concerning co-doped matrix decay, it follows a mono-exponential function represented by:

$$I(t) = I_0\, e^{\frac{-t}{\tau}} + C_0 \tag{6}$$

where I_0 and C_0 are constants and τ is lifetime of excited level. $\tau_{Gd,Eu} < \tau_{Gd}$ which indicates a $Gd^{3+} \rightarrow Eu^{3+}$ ET with an ET rate η_T equal to 19% calculated by using the following formula [7]:

$$\eta_T = 1 - \frac{\tau_{S,A}}{\tau_S} \tag{7}$$

Where $\tau_{S,A}$ and τ_S are S lifetimes respectively in co-doped and mono-doped matrices.

Table 1 S decay times and ET rates in samples

Sample	Decay time (ms)	η_T
YPO_4:Gd^{3+}	$\tau_{Gd} = 5.51$	19%
YPO_4:Gd^{3+},Eu^{3+}	$\tau_{Gd,Eu} = 4.45$	
YP_3O_9:Sm^{3+}	$\tau_{Sm} = 4.07$	28%
YP_3O_9:Sm^{3+},Eu^{3+}	$\tau_{Sm,Eu} = 2.95$	

Figure 13 (b) shows fluorescence decay curves of YP_3O_9:Sm^{3+}0.25% and YP_3O_9:Sm^{3+}0.25%, Eu^{3+}0.50% of $^4G_{5/2} \rightarrow {}^6H_{7/2}$ emission at 602 nm under excitation into $^4I_{9/2}$ level at 480 nm. YP_3O_9:Sm^{3+}0.25% decay follows a mono-exponential function with a decay time equal to 4.07 ms (Table 1). Generally, phosphors activated by Sm^{3+} ion have a long lifetime for low concentration [19]. YP_3O_9:Sm^{3+}0.25%, Eu^{3+}0.50% decay follows a bi-exponential function. The change of donor fluorescence decay profile is related to ET. The average decay time $\tau_{Sm,Eu}$ is smaller than τ_{Sm}, indicating the occur of $Sm^{3+} \rightarrow Eu^{3+}$ efficient ET with η_T equal to 28%.

It is known from the classical Foster–Dexter theory of ET between two electrostatically interacting entities, that the efficiency of ET depends critically on the distance between S and A ions and on the overlap factor [7, 21, 22]. Taking into account the fact that the transfer probability, in the case of dipole–dipole interaction, is proportional to D^{-6} (D being the S-A distance). In YPO_4, the ET rate is lower than that of YP_3O_9 although the minimal distance between RE^{3+} ions is equal to 0.3755 nm inYPO_4 [7] and it is in the order of 0.561 nm in YP_3O_9 [23].

Conclusion

This work is part of research of new visible QC phosphors. We have synthesized YPO_4 doped with Gd^{3+} and/or Eu^{3+} by hydrothermal method at low temperature and YP_3O_9 doped with Sm^{3+} and/or Eu^{3+} by ultraphosphate decomposition reaction at high temperature. The characterization by FTIR and XRD confirm the phase purity of powders. Under excitation at 394 nm using Xenon lamp, YPO_4:Eu^{3+}0.50% and YP_3O_9:Eu^{3+}0.50% showed an orange-red emission originating from $^5D_0$ to ^7F_J (J = 1–4) levels, and that of Y-monophosphate is the strongest. Also, under excitation at 404 nm, YP_3O_9:Sm^{3+}0.25% emits orange-red light corresponding to $^4G_{5/2} \rightarrow {}^6H_J$ (J = 5/2–11/2) transitions. Based on emission spectra, The only crystallographic site in YPO_4 is Centro-symmetric, whereas YP_3O_9 of four RE^{3+} sites is described to have an asymmetric nature. NRET from Gd^{3+} to Eu^{3+} and from Sm^{3+} to Eu^{3+} has been demonstrated in these matrices. The rates of $Gd^{3+} \rightarrow Eu^{3+}$ and $Sm^{3+} \rightarrow Eu^{3+}$ ET are respectively equal to 19% and 28%, despite the low concentrations. In addition, S lifetimes in YPO_4 is long. Thus, YPO_4:Gd^{3+}0.25%, Eu^{3+}0.50% is a luminescent material for UV excitation and YP_3O_9:Sm^{3+}0.25%, Eu^{3+}0.50% is a potential orange-red emitting phosphor for Hg-free fluorescent lamps and PDP. Further VUV measurements will be done on this polyphosphate in a near future research.

References

1. Dexter DL (1957) Possibility of luminescent quantum yields greater than unity. Phys Rev 108(3):630–633
2. Wegh RT, Donker H, Oskam KD, Meijerink A (1999) Visible quantum cutting in Eu^{3+}-doped gadolinium fluorides via downconversion. J Lumin 82:93–104
3. Hachani S, Moine B, El-akrmi A, Ferid M (2009) Luminescent properties of some ortho- and pentaphosphates doped with Gd^{3+}-Eu^{3+}: potential phosphors for vacuum ultraviolet excitation. Opt Mater 31:678–684
4. Zhang QY, Huang XY (2010) Recent progress in quantum cutting phosphors. Prog Mater Sci 55:353–427
5. Kahouadji B, Guerbous L, Boukerika A, Dolić SD, Jovanović DJ, Dramićanin MD (2017) Sol gel synthesis and pH effect on the luminescent and structural properties of YPO_4: Pr^{3+} nanophosphors. Opt Mater 70:138–143
6. Agrawal DK, Hummel FA (1980) The systems Y_2O_3-P_2O_5 and Gd_2O_3-P_2O_5. J Electrochem Soc 127:1550
7. Hachani S, Moine B, El-akrmi A, Ferid M (2010) Energy transfers between Sm^{3+} and Eu^{3+} in YPO_4, LaP_5O_{14} and LaP_3O_9 phosphates. Potential quantum cutters for red emitting phosphors. J Lumin 130:1774–1783
8. Lai H, Du Y, Zhao M, Sun K, Yang L (2014) CTAB assisted hydrothermal preparation of YPO_4: Tb^{3+} with controlled morphology, structure and enhanced photoluminescence. Mat Sci Eng B 179:66–70
9. Wang D, Wang Y, Shi Y (2011) Photoluminescence properties of Eu^{3+} in $Y(PO_3)_3$ under VUV excitation. J Lumin 131:1154–1157
10. Ternane R, Ferid M, Panczer G, Trabelsi-Ayadi M, Boulon G (2005) Site-selective spectroscopy of Eu^{3+}-doped orthorhombic lanthanum and monoclinic yttrium polyphosphates. Opt Mater 27: 1832–1838
11. Bagieu-Beucher M, Tranqui D (1970) Rare earth and yttrium ultraphosphates TP_5O_{14}. Bull Soc fr Miner 93:505–508
12. Yahiaoui Z, Hassairi MA, Dammak M (2017) Synthesis and optical spectroscopy of YPO_4:Eu^{3+} orange-red phosphors. J Electron Mater 46:4765–4773
13. Rambabu U, Amalnerkar DP, Kale BB, Buddhudu S (2001) Optical properties of $LnPO_4$:Tb^{3+} (ln = Y, La and Gd) powder phosphors. Mater Chem Phys 70:1–6
14. Yuan JL, Zhang H, Zhao JT, Chen HH, Yang XX, Zhang GB (2008) Synthesis, structure and luminescent properties of $Lu(PO_3)_3$. Opt Mater 30:1369–1374
15. Dieke GH (1968) Spectra and energy levels of rare earth ions in crystals. Interscience Pub, New York
16. K. Binnemans K (2015) Interpretation of europium(III) spectra. Coord Chem Rev 295: 1–45
17. Mbarek A (2009) Caractérisations structurales et optiques d'ultraphosphates de terres rares LnP_5O_{14} (Ln= La, Gd et Y) synthétisés par la voie solide et par le procédé sol-gel. Doctoral dissertation, University of Blaise Pascal-Clermont-Ferrand II
18. Lin C, Song Y, Gao F, Zhou X, Sheng Y, Shi Z, Zou H (2015) Luminescent properties and energy transfer of Gd^{3+}/Eu^{3+} co-doped high uniform meso-silica nanorods. J Lumin 158:456–463
19. Yu R, Noh HM, Moon BK, Choi BC, Jeong JH, Lee HS, Jang K, Yi SS (2014) Photoluminescence characteristics of Sm^{3+} doped $Ba_3La(PO_4)_3$ as new orange-red emitting phosphors. J Lumin 145:717–722
20. Yaiphaba N, Ningthoujam RS, Singh NS, Vatsa RK, Singh NR (2010) Probing of inversion symmetry site in Eu^{3+}-doped $GdPO_4$ by luminescence study: concentration and annealing effect. J Lumin 130:174–180
21. Forster T (1948) Intermolecular energy migration and fluorescence. Ann Phys (Leipzig) 2:55
22. Dexter DL (1953) A theory of sensitized luminescence in solids. J Chem Phys 21:836–850
23. Ternane R, Ferid M, Guyot Y, Trabelsi-Ayadi M, Boulon G (2008) Luminescent properties of Yb-doped monoclinic yttrium polyphosphates. J Lumin 128:387–393